Available online at www.sciencedirect.com
ScienceDirect
Chemical Physics 341 (2007) 29–36
Chemical Physics
www.elsevier.com/locate/chemphys

Two-dimensional electronic correlation spectroscopy of the $n\pi^*$ and $\pi\pi^*$ protein backbone transitions: A simulation study

Zhenyu Li, Darius Abramavicius, Wei Zhuang, Shaul Mukamel *

Department of Chemistry, University of California, Irvine, CA 92697, USA

Received 20 March 2007; accepted 30 March 2007
Available online 19 April 2007

Abstract

The two-dimensional (2D) photon echo spectrum of the amide ultraviolet (UV) bands of proteins are simulated. Two effective exciton Hamiltonian parameter sets developed by Woody and by Hirst, which predict similar CD spectra, may be distinguished by their very different 2DUV spectra. These differences are enhanced in specific configurations of pulse polarizations which provide chirality-induced signals.
Published by Elsevier B.V.

Keywords: 2DUV; CD; Photon echo

1. Introduction

Ultraviolet (UV) circular dichroism (CD) [1,2] and resonance Raman spectroscopy [3–7] are widely used for probing the secondary structure and folding dynamics of proteins. Two-dimensional (2D) coherent third-order optical techniques can reveal fine details, unavailable from linear spectroscopy [8]. Significant progress has been made over the past decade in developing 2D infrared spectroscopy (2DIR) based on the heterodyne detection of three-pulse photon echoes [9,10] towards the study of amide vibrations [11–15]. By probing the electronic transitions, 2DUV techniques can complement 2DIR. In this paper, we focus on the theoretical modeling of 2DUV photon echoes of protein backbone electronic excitations primarily $n\pi^*$ (220 nm) and $\pi\pi^*$ (190 nm), with two additional shorter-wavelength excitations, $\pi_b\pi^*$ and $n'\pi^*$ transitions.

Much theoretical effort has been devoted to the modeling of CD spectra of proteins [16–29]. A dipole-interaction model developed by Applequist et al. [19,20,22] yields almost quantitative agreement with experiment for the $\pi\pi^*$ transition. This model excludes the $n\pi^*$ excitation, whose transition dipole vanishes by symmetry. Woody and coworkers have obtained a set of parameters for both the $n\pi^*$ and $\pi\pi^*$ CD by semiempirical electronic structure calculations combined with fitting to experiments [17,21,24]. Hirst et al. [26,27,29] have recently reported an *ab initio* model for protein CD. This model is based on a high level CASPT2/RF quantum chemistry calculation on excited states of a small prototype molecule *N*-methylacetamide (NMA). Solvent effects were included by an implicit continuum model approximation.

Fluctuations are not explicitly included in these models. Instead, the one-exciton energies and corresponding rotational strengths are calculated by diagonalizing the exciton Hamiltonian. Gaussian broadening is then added to all optical transitions. Recently, by combining time-dependent density-functional theory (TDDFT) and molecular dynamics (MD), Frelek et al. [30] have simulated the CD spectra of β-lactam averaging over conformational fluctuations of molecular geometries.

In this paper, we show how the Woody and Hirst model Hamiltonians for protein backbone electronic excitations, which provide an equally good fit for the CD spectra,

* Corresponding author. Tel.: +1 949 824 7600.
E-mail address: smukamel@uci.edu (S. Mukamel).

0301-0104/$ - see front matter Published by Elsevier B.V.
doi:10.1016/j.chemphys.2007.03.029

may be distinguished by 2DUV. Gaussian fluctuations are added to site energies, and the spectra are averaged over the corresponding ensembles. The 2DUV technique provides a more sensitive probe than CD for protein structure. All theoretical modelings discussed in this paper have been carried out using the spectroscopy simulation package SPECTRON [43]. We present the fluctuating exciton Hamiltonian model in Section 2, and some test calculations of NMA and myoglobin in Section 3. UV spectra of a 17 residue helix are then predicted with this model in Section 4. Finally, we conclude in Section 5.

2. The fluctuating exciton Hamiltonian

To study electronic transitions in large proteins, we use a Frenkel-exciton Hamiltonian constructed from the peptide chromophore units.

$$H_0 = \sum_{i\mu} \epsilon_{i\mu} \widehat{B}^{\dagger}_{i\mu} \widehat{B}_{i\mu} + \sum_{i\mu \neq jv} J_{i\mu,jv} \widehat{B}^{\dagger}_{i\mu} \widehat{B}_{jv} \tag{1}$$

where $\widehat{B}^{\dagger}_{i\mu}$ and $\widehat{B}_{i\mu}$ are the exciton creation and annihilation operators for the excited state μ of peptide i, with energy $\epsilon_{i\mu}$. $J_{i\mu,jv}$ is the coupling between state μ of unit i and state v of unit j. NMA is often used to compute the Hamiltonian parameters for a peptide unit, and has been widely studied both experimentally and theoretically [31,33,32,34–38]. We have used two sets of parameters for $\epsilon_{i\mu}$ and $J_{i\mu,jv}$. One from Woody and Sreerama (WS) which includes three excited states per amide ($n\pi^*$, $\pi\pi^*$, and $\pi_b\pi^*$) [24], and the other from Besley and Hirst (BH) with four excited states ($n\pi^*$, $\pi\pi^*$, $\pi_b\pi^*$ and $n'\pi^*$) [26]. We have used an improved parametrization of the WS and BH Hamiltonian kindly provided by both authors.

In our simulations, we have added fluctuations to these two model Hamiltonians. We first consider fluctuations of the coupling $J_{i\mu,jv}$ (off-diagonal fluctuations). In both WS and BH Hamiltonians, the couplings are obtained by assuming electrostatic interactions between transition charge densities (TCD).

$$J_{i\mu,jv} = \int \frac{\rho_{i0\mu}(\mathbf{r}_i)\rho_{j0v}(\mathbf{r}_j)}{4\pi\epsilon_0 r_{ij}} \, \mathrm{d}\mathbf{r}_i \, \mathrm{d}\mathbf{r}_j \tag{2}$$

where $\rho_{i0\mu}$ is TCD of peptide i between the ground state and excited state μ. The integral can be eliminated by representing the TCD as a sum of point charges (the monopole approximation) [17,23,24,26]. A set of monopoles is assigned to each chromophore, and an MD trajectory in water was generated. Geometry fluctuations along the MD trajectory change the distances between the monopoles, and hence the couplings. Other contributions to off-diagonal fluctuations, such as electrostatic interaction between solvent and solute, are neglected.

To compute the site energy $\epsilon_{i\mu}$ (diagonal) fluctuations, we should recalculate the transition energy by repeating the electronic structure calculation for each MD trajectory snapshot. This was done in Ref. [30] for a small system, but is not computationally feasible for large polypeptides. We thus added Gaussian random fluctuations to the site energies. We denote these fluctuating Hamiltonians as WS and BH respectively (note that in the original WS and BH models there are no energy fluctuations).

The total Hamiltonian is

$$H = H_0 + H_1 \tag{3}$$

where H_1 is the interaction between the protein and the classical optical field. Using the minimal-coupling Hamiltonian, we have [49]

$$H_1 = -\frac{1}{c} \int \mathrm{d}\mathbf{r} \hat{\mathbb{J}} \cdot \mathbb{A} \tag{4}$$

where $\mathbb{A}$ is the vector potential and $\mathbb{J}$ is the induced current operator

$$\widehat{\mathbb{J}}(\mathbf{r}) = \sum_{i\mu} (\bar{\mathbf{j}}^*_{i\mu}(\mathbf{r}) \widehat{B}^{\dagger}_{i\mu} + \bar{\mathbf{j}}_{i\mu}(\mathbf{r}) \widehat{B}_{i\mu}) \tag{5}$$

$\bar{\mathbf{j}}_{i\mu}$ is the transition current density from ground state to excited state the μ of peptide i. The transition current density is related to electric transition dipole $\bar{\boldsymbol{\mu}}$, magnetic transition dipole $\bar{\mathbf{m}}$, and the electric transition quadrupole $\overline{\mathbf{Q}}$.

$$\bar{\mathbf{j}}_{i\mu}(\mathbf{k}) = i\omega\bar{\boldsymbol{\mu}}_{i\mu} - \omega\overline{\mathbf{Q}}_{i\mu} \cdot \mathbf{k} + ic\mathbf{k} \times \bar{\mathbf{m}}_{i\mu} \tag{6}$$

where $\bar{\mathbf{j}}_{i\mu}(\mathbf{k})$ is the spatial Fourier transform of $\bar{\mathbf{j}}_{i\mu}(\mathbf{r})$. Both dipole and magnetic dipole are available in the WS and BH Hamiltonians. The linear absorption and CD are independent on the transition quadrupoles. Our test calculations with TDDFT transition quadrupoles indicated that they make only a minor change to the 2DUV spectra. The transition quadrupole was thus neglected in this study.

3. Test calculations on NMA and myoglobin

To test our fluctuating exciton Hamiltonian, we have first calculated the UV absorption spectrum of NMA. NMA with its geometry optimized in gas phase at B3LYP/aug-cc-pVDZ level [45] is embedded in a cubic TIP3P water box with a size of $36 \times 36 \times 36$ Å^3. The CHARMM22 force field [46] is used to perform an MD simulation with the NAMD package [47]. To release the internal tension, 5000 minimization steps were first performed, followed by a 200 ps heat-up at 1 fs time step from zero to 300 K. The system is then equilibrated under NPT ensemble with 1 fs timestep for 1 ns to obtain the right system density and box size. The final box size 34.88 Å is obtained by averaging the last 1000 steps of the NPT trajectory. A 4 ns NVE equilibration is then run. At this stage, the water molecules are held rigid using the SHAKE algorithm [48], and a 2 fs time step is thus used. Finally, a 1 ns trajectory is recorded by applying the NVE ensemble with a 1 fs time step. The structure is saved in 50 fs increments.

Fifteen thousand snapshots of the classical MD trajectory were used to sample the distribution of couplings. The variance of Gaussian fluctuation (σ) is fitted to recover the CD bandwidth (HWHM, Γ) reported in the original WS and BH simulations ($\sigma = \Gamma/\sqrt{2\ln 2}$). In WS,

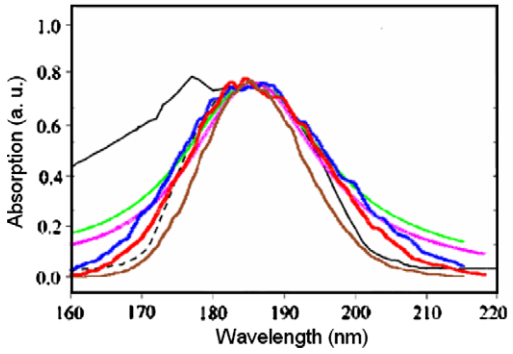

Fig. 1. Experimental (black) UV absorption of NMA in water [51] and simulated spectra WS (red), BH (blue), WS′ (pink), BH′ (green), and BHM (brown). For better comparison with experiment, the simulated WS and WS′ spectra are blueshifted by 4 nm, and the BH, BH′, and BHM spectra are blueshifted by 7 nm. The spectra are scaled to have the same peak height. (For interpretation of colour representation in this figure legend the reader is referred to the web version of this article.)

$\Gamma = 2174.4$, 3143.3, and 3743.6 cm^{-1} for $n\pi^*$, $\pi\pi^*$, and $\pi_b\pi^*$, respectively. For BH, $\Gamma = 3137.3$, 3391.8, 7582.7, and 8345.2 cm^{-1} for $n\pi^*$, $\pi\pi^*$, $\pi_b\pi^*$ and $n'\pi^*$, respectively. An additional homogeneous dephasing rate $\gamma = 150$ cm^{-1} was added to all transitions in both models. This small width did not affect the spectra notably, but reduces the number of snapshots needed for inhomogeneous averaging. The calculated spectra are shown in Fig. 1. The broadening parameters chosen in the WS and BH Hamiltonians to fit protein CD slightly overestimate the absorption linewidth. For comparison, we also performed a simulations where diagonal fluctuations are neglected, but a large homogeneous dephasing γ equal to Γ (the linewidth parameters in the original WS and BH models) is added. We call the two simulations WS′ and BH′. As shown in Fig. 1, the Gaussian profile provides a better fit to experiment.

We had further tested our protocol by a CD simulation of myoglobin. The initial crystal structure was downloaded from the PDB database (code: 1MBN). The MD trajectory was generated using a similar protocol used for NMA in water. 1000 snapshots were used to generate the CD spectra, as shown in Fig. 2. The spectra are scaled to have the same positive peak height. Myoglobin is mainly a α-helix, and its most characteristic CD feature is the negative peak at ~220 nm. Generally, both WS and BH Hamiltonians reproduce the experimental CD. It is interesting to note

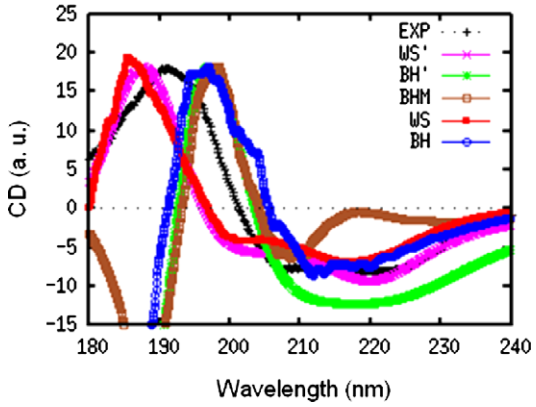

Fig. 2. Experimental (black) and simulated CD spectra of myoglobin from WS (red), BH (blue), WS′ (pink), BH′ (green), and BHM (brown) models. All spectra are scaled to have the same positive peak height. (For interpretation of colour representation in this figure legend the reader is referred to the web version of this article.)

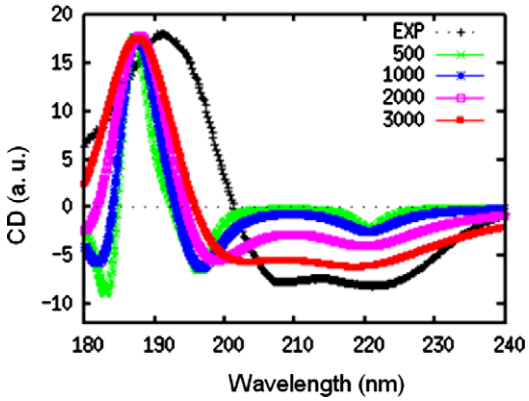

Fig. 3. Experimental (black) and simulated WS′ CD spectra of myoglobin, with different homogeneous dephasing rates $\gamma = 500$ (green), 1000 (blue), 2000 (pink), and 3000 (red) cm^{-1}. All spectra are scaled to have the same positive peak height. (For interpretation of colour representation in this figure legend the reader is referred to the web version of this article.)

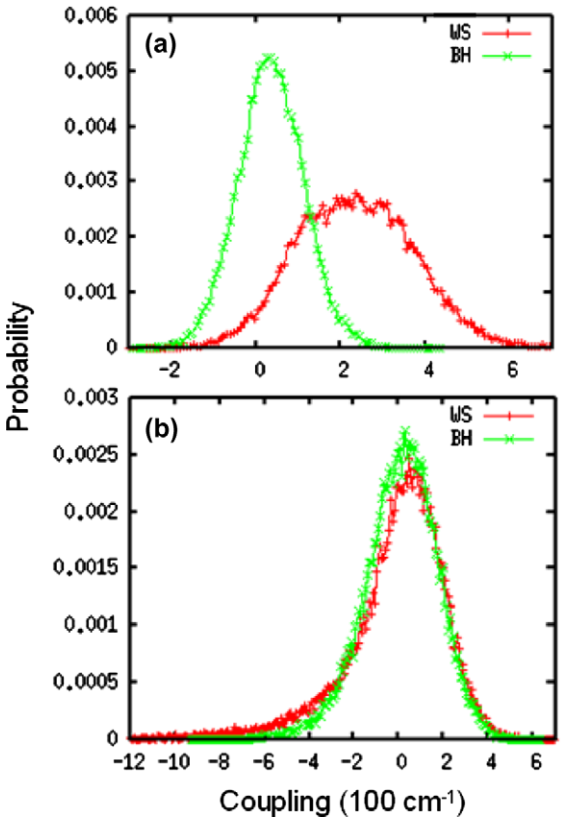

Fig. 4. Coupling distributions for WS (red) and BH (green) Hamiltonians. (a) Coupling between the $n\pi^*$ and $\pi\pi^*$ transitions on the same peptide and (b) coupling between $\pi\pi^*$ transitions of nearest-neighbor peptides. (For interpretation of colour representation in this figure legend the reader is referred to the web version of this article.)

that the WS Hamiltonian gives a redshifted absorption but a blueshifted CD compared to experiment. The difference between WS and WS′ is very small. However, CD using BH model better fits experiment than using BH′ model. We notice that Besley et al. have improved the CD fit by only including the first two states ($n\pi^*$ and $\pi\pi^*$) [26].

The positive and negative CD peaks can interfere, making the spectrum very sensitive to the bandwidth parameter. This is illustrated in the following simulations. In Fig. 3, we plot the CD spectra of myoglobin calculated using the WS′ model with different γ. We assume the same γ for all the three transitions in the WS Hamiltonian. The characteristic 220 nm negative peak of α-helix is much weaker than experiment for γ smaller than 1000 cm^{-1}.

We had also attempted to obtain diagonal fluctuations directly from the MD trajectory. In infrared spectra, electrostatic maps have been successfully used to avoid the repeated electronic structure calculations [39–44]. Since in electronic transitions, the site energies strongly depend on the geometric parameters [38], we constructed a TDDFT map which depends on the external electric field as well as the geometry of NMA.

$$\omega_i^{\mathrm{MAP}} = \omega_i^0 + \sum \alpha_i^{\mathrm{X}} E_i^{\mathrm{X}} + \sum \beta_n (\xi_n - \bar{\xi}_n)$$
$$\mathrm{X} = \mathrm{C}, \mathrm{O}, \mathrm{N}, \mathrm{H};\ i = x, y, z;\ \ n = 1, 4 \qquad (7)$$

where E^{X} is the electric field at atom X, ξ_n are geometric parameters (C–O and C–N bond length, C–O–N angle, and O–C–N–H dihedral angle), and $\bar{\xi}_n$ is the corresponding mean value in the MD trajectory. Fluctuations calculated from this map along the trajectory were then added to the BH Hamiltonian. This BH-Map (BHM) gives slightly narrower absorption line compared to experiment (Fig. 1). The BHM CD is almost identical to BH for the positive $\pi\pi^*$ peak, but its $n\pi^*$ negative peak is too weak compared to experiment (Fig. 2). Additional effort will be required to improve this map.

4. UV spectra of a 17-residue polypeptide

4.1. Linear spectra: absorption and CD

UV spectra were simulated for a 17-residue α-helix polypeptide Ac-$YA_2KA_4KA_4KA_2H$–NH_2 (YKKKH17) in water. A similar MD simulation strategy as described for

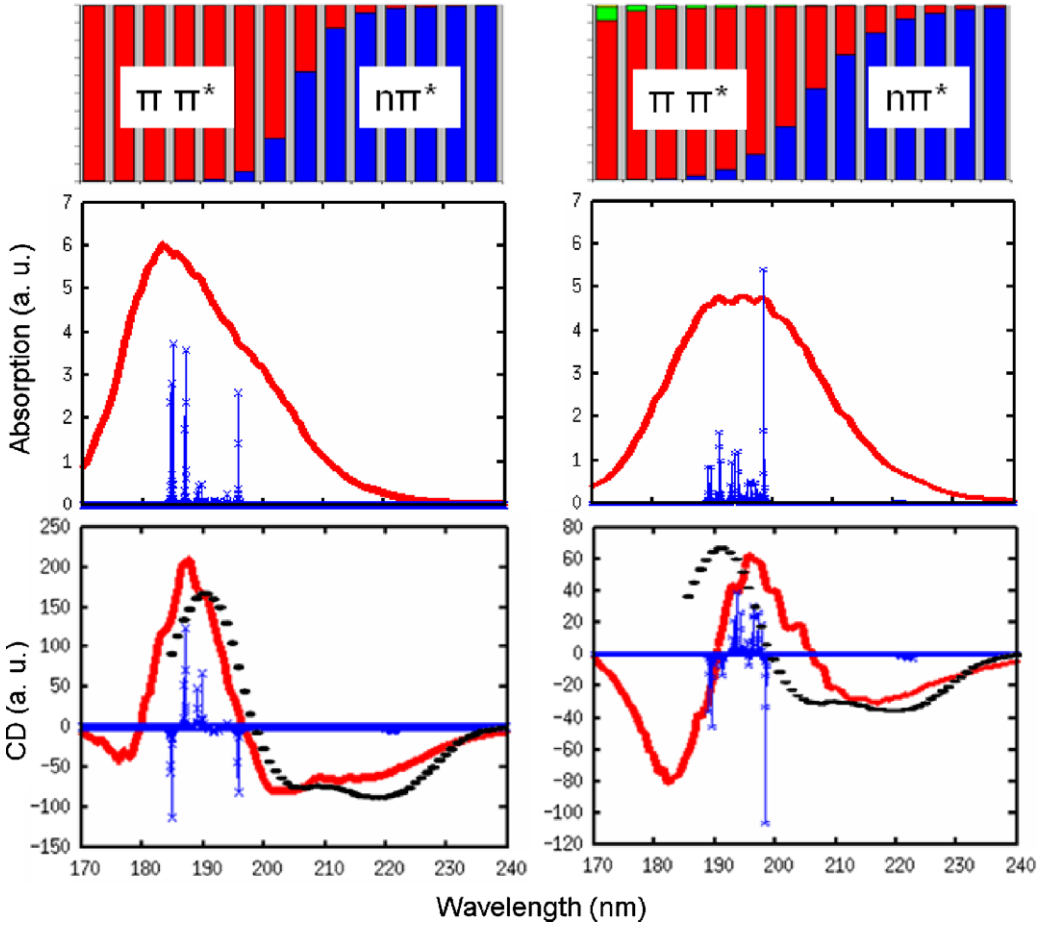

Fig. 5. Top: wavelength-dependent exciton decomposition for YKKKH17 to different transitions $n\pi^*$ (blue), $\pi\pi^*$ (red), $\pi_b\pi^*$ (green), and $n'\pi^*$ (yellow). Linear absorption (middle) and CD (bottom) from WS (left) and BH (right) models. Stick spectra (green) are obtained from a single snapshot with $\gamma = 5$ cm^{-1}. The black dot curve is experimental CD for a similar 19-residue helix [52]. (For interpretation of colour representation in this figure legend the reader is referred to the web version of this article.)

NMA in water was used, and the initial geometry is taken from a previous study [43]. In Fig. 4, we plot the resulting distributions of intra-chromophore and inter-chromophore couplings. The WS and BH Hamiltonians yield different distributions for couplings between $n\pi^*$ and $\pi\pi^*$ transitions on the same peptide. Both can be fitted to a Gaussian, with mean 231 (34.6) cm^{-1} and variance $\sigma = 143.5$ (77.0) cm^{-1} for WS (BH). The WS Hamiltonian predicts a much larger intra-chromophore $n\pi^*$–$\pi\pi^*$ couplings compared to BH. The nearest-neighbor inter-chromophore $\pi\pi^*$ couplings for the two Hamiltonians are very similar, but have a non-Gaussian distribution. Both show a long tail for lower couplings. The variance of the nearest-neighbor inter-chromophore $\pi\pi^*$ coupling is 160 cm^{-1}.

The calculated linear absorption and CD are displayed in Fig. 5. 2000 snapshots are used in inhomogeneous averaging. As in NMA, the absorption shows a single broad peak. The CD spectra of YKKKH17 are very similar to myoglobin, with a strong positive peak at about 190–200 nm, and a weaker negative peak at 220 nm. Exciton decomposition [15] was calculated by adding the squares of the eigenstate coefficients for different transitions. This is shown in the top panel of Fig. 5. The positive CD peak mainly comes from the $\pi\pi^*$ transitions, and the negative one comes from the $n\pi^*$ transitions and tail of the $\pi\pi^*$ transitions. We notice a contribution from $\pi_b\pi^*$ transition at the blue end of the spectra for the BH Hamiltonian, but not for WS, where the intra-chromophore $\pi\pi^*$–$\pi_b\pi^*$ coupling is neglected.

We also show the stick spectra for absorption and CD in Fig. 5, obtained using $\gamma = 5$ cm^{-1} in the WS and BH Hamiltonians for a single snapshot at the middle of the trajectory. The $n\pi^*$ and $\pi\pi^*$ transitions are now well separated, and the $\pi\pi^*$ is much stronger than the $n\pi^*$ band. The WS and BH Hamiltonians show different patterns for the $\pi\pi^*$ transition band. For the WS Hamiltonian, the states at both the red and the blue band edge are much stronger than mid-band states. However, BH does not show a strong blue edge states in the $\pi\pi^*$ transition band. The difference between the two Hamiltonians as seen in the stick spectra is masked in the absorption and CD by the large broadening. By inspecting the eigenvectors, we find that the strong red edge state for both WS and BH Hamiltonians is an in-phase linear combination of the $\pi\pi^*$ transitions of all peptides, implying that this state is delocalized over the entire polypeptide.

To explore the degree of exciton localization, we have examined the corresponding participation ratios (PR) [53]. Considering an eigenstate e, whose wavefunction is a superposition of localized states on the ith peptide unit with coefficients ψ_{ei}, its PR is defined as $W_e = (\sum_i |\psi_{ei}|^4)^{-1}$. For a localized state, $W_e = 1$, whereas when the state e is completely delocalized, and ψ_{em} has equal $1/\sqrt{n}$ contributions from all n local modes, $W_e = n$. Here, the localized basis set runs over all excited states μ on the same peptide, i. e. $\psi_{ei} = \sqrt{\sum_\mu \psi_{ei\mu}^2}$. The PR of the strong red-edge $\pi\pi^*$ state in WS and BH stick spectra is 12.4 and 9.9, respectively.

Fig. 6 shows the PR distribution (PRD) of eigenstates in a given frequency range (± 500 cm^{-1} binning was used) for the WS and BH models. As expected, the states become more localized with disorder. The largest average PR is about 3.0 at 53,000 cm^{-1}, which should be mainly due to the $\pi\pi^*$ transition. The $\pi\pi^*$ states also have a larger standard deviation of PR. Although the PRD suggest that $\pi\pi^*$ states are more delocalized than $n\pi^*$, a more rigorous measure is provided by sensitivity analysis (SA) [15]. We introduce a small perturbation to the energies of a specific transition, e.g. $n\pi^*$, in Hamiltonian. The sensitivity signal (SAS) is then given by the absolute value of the difference between the PRD of the perturbed and unperturbed systems. $n\pi^*$ SAS is mainly distributed in the low-frequency regime, which have low PR in PRD. The high-frequency part with higher PR is mainly from $\pi\pi^*$. This can also be illustrated by PR-dependent exciton decomposition, which clearly shows that in high PR range, the $\pi\pi^*$ dominates. Combining the PRD, SAS, and exciton decomposition, we conclude that the main difference between the WS and BH Hamiltonians is that $n\pi^*$ is more delocalized in the latter.

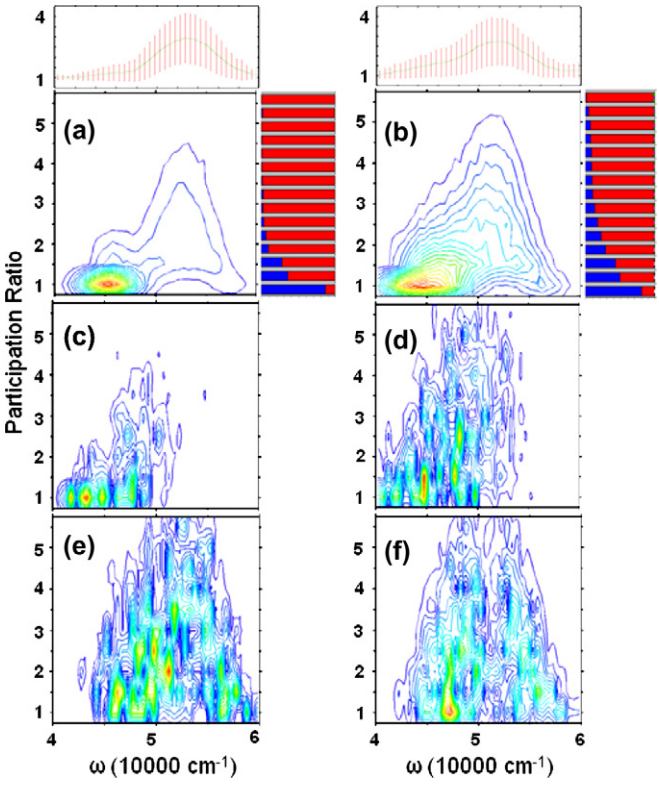

Fig. 6. The exciton participation ratio distribution (PRD) binned over frequency for (a) WS and (b) BH Hamiltonians. Top marginal: the mean PR (line) and standard deviation (bars). Right marginal: the PR-dependent exciton decomposition to different transitions, with the same color scheme as in Fig. 5. Sensitivity analysis for $n\pi^*$ transitions for (c) WS and (d) BH Hamiltonians. (e) and (f) are for $\pi\pi^*$.

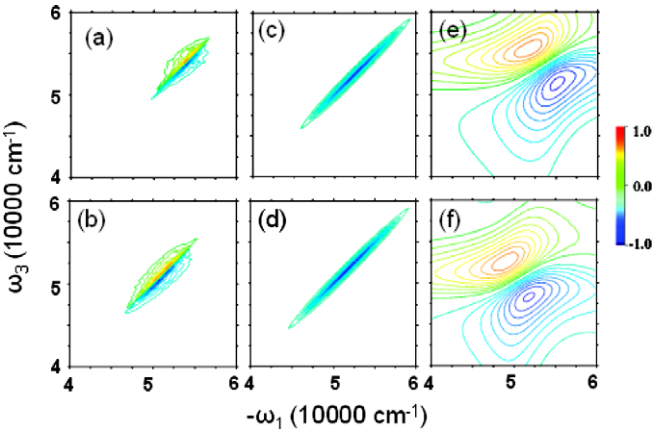

Fig. 7. Imaginary part of $xxxx(zzzz)$ 2DPE spectra (a) WS and (b) BH. (c) WS with the couplings turned off, (d) BH with couplings turned off, (e) WS′ and (f) BH′.

4.2. 2DUV spectra

A four wave mixing experiment uses three pulses with wavevectors $\mathbf{k}_1$, $\mathbf{k}_2$, and $\mathbf{k}_3$, which interact with the protein to generate a coherent signal in one of the direction $\mathbf{k}_s = \pm\mathbf{k}_1 \pm \mathbf{k}_2 \pm \mathbf{k}_3$. There are three time delays (t_1, t_2, and t_3) between the three incoming pulses and the signal pulse. We will focus on the photon echo (PE) signal generated in the phase matching direction $\mathbf{k}_I = -\mathbf{k}_1 + \mathbf{k}_2 + \mathbf{k}_3$, and set $t_2 = 0$. 2D correlation plots of the signals are plotted as Fourier transforms with respect to t_1 and t_3 (Eq. 17 of Ref. [49]). Different polarization and wavevector configurations are denoted by $\mu_4\mu_3\mu_2\mu_1(\alpha_4\alpha_3\alpha_2\alpha_1)$, where μ_i is the polarization direction of field i and α_i is its wavevector direction. $\bar{\alpha}$ denote minus α direction.

Simulations were performed with the NEE method [50] as implemented in the SPECTRON code. To speed up the

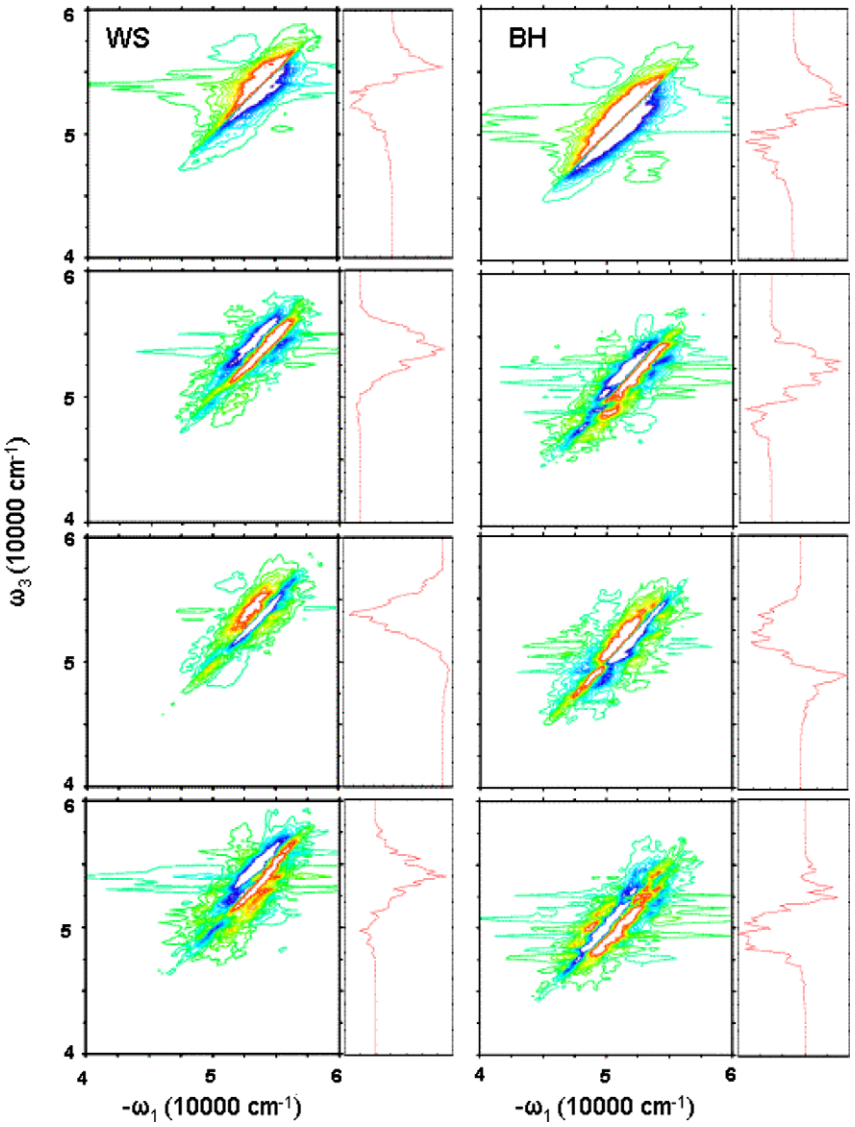

Fig. 8. Simulated 2D photon echo signals. Left column WS model; right column BH model. From top to bottom, imaginary part of $xxxx(zzzz)$, and real part of $xxxy(zzzz), xxxy(zy\bar{y}\bar{z})$, and xxyz(zzxx). Maximum peak is truncated at 20% to better show the weaker features. Right marginals: diagonal cut of the 2D spectra. The same color scale is used as in Fig. 7.

calculations, a truncation has been applied to the NEE scattering matrix [43], with cutoff parameter $\eta = 0.54$, which does not distort the spectrum. The simulated $xxxy(zzzz)$ component of 2DPE spectra obtained from 8000 snapshots are depicted in Fig. 7.

As shown in the previous section, the couplings (a few hundred cm^{-1}) are relatively small compared to the site energy fluctuations (more than 2000 cm^{-1}). In the middle panels of Fig. 7, we display the spectra with coupling turned off. The very different spectra indicate that the 2DUV spectra are very sensitive to the coupling. Cross peaks do exist, although they are very close to the diagonal line since couplings are weak. The homogeneous WS′ and BH′ models (right column) also give very different 2DUV.

The nonchiral $xxxy(zzzz)$ 2DPE signals are similar for the WS and BH Hamiltonians. Upon closer examination, we can see some differences. In Fig. 8, we truncate the strongest peak magnitude at 20%. The BH model then shows an additional cross peak at the right-bottom corner.

Chirality induced (CI) components of 2DPE show larger differences between WS and BH Hamiltonians. For the $xxxy(zzzz)$ component, BH gives additional feature around 48000 cm^{-1}. This can be clearly seen from the diagonal spectra. The WS diagonal spectrum gives only a very weak negative peak, but the BH diagonal spectrum shows a notable negative feature. For the $xxxy(zy\bar{y}\bar{z})$ component, BH shows some additional positive features. For $xxyz(zzxx)$, the difference between WS and BH models is even larger. Both WS and BH models give a three-strip pattern, but the WS pattern is negative–positive–positive, while the BH pattern is positive–negative–positive. The diagonal cut of WS spectrum is primarily positive, and the BH diagonal spectrum is negative.

In the visible and IR regions, γ and σ are comparable. However, in the UV region, inhomogeneous disorder is much larger than the homogeneous dephasing rate ($\sigma \gg \gamma$), which makes the 2DPE spectra narrow along the diagonal line. This is different from our previous calculation [49], which used a much larger dephasing γ. At the same time, in both WS and BH Hamiltonians, disorder is also much larger than the coupling. Therefore, all cross-peaks are closely packed near the diagonal peak. In the current two model Hamiltonians, the coupling between nearest peptides is electrostatic. A more realistic nearest-neighbor coupling model, which includes charge overlap and exchange, may predict a larger nearest-neighbor coupling, and the cross peaks may be shifted from the diagonal peaks, and better resolved.

5. Conclusions

2D spectra of two effective electronic model Hamiltonians for protein backbone $n\pi^*$ and $\pi\pi^*$ electronic excitation were compared. Off-diagonal fluctuations are simulated by an MD trajectory, supplemented with Gaussian diagonal fluctuations. The signatures of fluctuations in two-dimensional techniques are identified. As seen in the stick spectra, the two Hamiltonians have different exciton structures, but this difference obscured by the broad linewidth. Our results demonstrate that 2DUV, especially CI 2DPE, gives additional information. Different model Hamiltonians, which agree for linear UV techniques (absorption and CD), may be distinguished by the 2D spectra.

Acknowledgements

This work was supported by the National Institutes of Health Grant GM59230 and the National Science Foundation Grant CHE-0446555. We thank Professor Robert W. Woody and Professor Jonathan D. Hirst for providing us the latest version of their Hamiltonian parameters, and for helpful discussions. This paper is dedicated to Douwe Wiersma for his pioneering work on developing coherent nonlinear spectroscopy in the condensed phase.

References

[1] K. Nakanishi, N. Berova, R.W. Woody, Circular Dichroism Principles and Applications, VCH, New York, 1994.
[2] G.D. Fasman, Circular Dichroism and the Conformational Analysis of Biomolecules, Plenum, New York, 1996.
[3] I.K. Lednev, A.S. Karnoup, M.C. Sparrow, S.A. Asher, J. Am. Chem. Soc. 121 (1999) 8074.
[4] I.K. Lednev, A.S. Karnoup, M.C. Sparrow, S.A. Asher, J. Am. Chem. Soc. 123 (2001) 2388.
[5] S.A. Asher, A. Mikhonin, S. Bykov, J. Am. Chem. Soc. 126 (2004) 8433.
[6] Z. Ahmed, I.A. Beta, A.V. Mikhonin, S.A. Asher, J. Am. Chem. Soc. 127 (2004) 10943.
[7] A.V. Mikhonin, S.A. Asher, J. Am. Chem. Soc. 128 (2006) 13879.
[8] S. Mukamel, Principles of Nonlinear Optical Spectroscopy, Oxford University Press, New York, 1995.
[9] W.H. Hesselink, D.A. Wiersma, Chem. Phys. Lett. 56 (1978) 227.
[10] E.T.J. Nibbering, D.A. Wiersma, K. Duppen, Chem. Phys. 183 (1994) 167.
[11] Y. Tanimura, S. Mukamel, J. Chem. Phys. 99 (1993) 9496.
[12] M.C. Asplund, M.T. Zanni, R.M. Hochstrasser, Proc. Natl. Acad. Sci. USA 97 (2000) 8219.
[13] S. Mukamel, Ann. Rev. Phys. Chem. 51 (2000) 691.
[14] J.B. Asbury, T. Steinel, C. Stromberg, K.J. Gaffney, I.R. Piletic, A. Goun, M.D. Fayer, Phys. Rev. Lett. 91 (2003) 237402.
[15] W. Zhuang, D. Abramavicius, S. Mukamel, Proc. Natl. Acad. Sci. USA 102 (2005) 7443.
[16] W. Moffitt, J. Chem. Phys. 120 (1956) 10938.
[17] R.W. Woody, J. Chem. Phys. 49 (1968) 4797.
[18] P.M. Bayley, E.B. Nielsen, J.A. Schellman, J. Phys. Chem. 73 (1969) 228.
[19] J. Applequist, K.R. Sundberg, M.L. Olson, L.C. Weiss, J. Chem. Phys. 70 (1979) 1240.
[20] K.A. Bode, J. Applequist, J. Phys. Chem. 100 (1996) 17825.
[21] G. Kurapkat, P. Kruger, A. Wollmer, J. Fleischhauer, B. Kramer, E. Zobel, A. Koslowski, H. Botterweck, R.W. Woody, Biopolymers 41 (1997) 267.
[22] K.A. Bode, J. Applequist, J. Am. Chem. Soc. 120 (1998) 10938.
[23] J.D. Hirst, J. Chem. Phys. 109 (1998) 782.
[24] R.W. Woody, N. Sreerama, J. Chem. Phys. 111 (1999) 2844.
[25] J.D. Hirst, N.A. Besley, J. Chem. Phys. 111 (1999) 2846.
[26] N.A. Besley, J.D. Hirst, J. Am. Chem. Soc. 121 (1999) 9636.
[27] D.M. Rogers, J.D. Hirst, J. Phys. Chem. A 107 (2003) 11191.
[28] M.T. Oakley, B.M. Bulheller, J.D. Hirst, Chirality 18 (2006) 340.
[29] M.T. Oakley, J.D. Hirst, J. Am. Chem. Soc. 128 (2006) 12414.

[30] J. Frelek, P. Kowalska, M. Masnyk, A. Kazimierski, A. Korda, M. Woznica, M. Chmielewski, F. Furche, Chem. Eur. J. (2007) DOI:10.1002/chem.200700127.
[31] K. Kaya, S. Nakagura, Theor. Chim. Acta 7 (1967) 117.
[32] L.B. Clark, J. Am. Chem. Soc. 117 (1995) 7974.
[33] E.B. Nielsen, J.A. Schellman, J. Phys. Chem. 71 (1967) 2297.
[34] L.E. Nitzsche, E.R. Davidson, J. Am. Chem. Soc. 100 (1978) 7201.
[35] L. Serrano-Andres, M.P. Fulscher, J. Am. Chem. Soc. 118 (1996) 12190.
[36] J.D. Hirst, D.M. Hirst, C.L. Brooks, J. Phys. Chem. A 101 (1997) 4821.
[37] N.A. Besley, J.D. Hirst, J. Phys. Chem. A 102 (1998) 10791.
[38] N.A. Besley, M.T. Oakley, A.J. Cowan, J.D. Hirst, J. Am. Chem. Soc. 126 (2004) 13502.
[39] S. Ham, J.H. Kim, H. Lee, M.H. Cho, J. Chem. Phys. 118 (2003) 3491.
[40] J.R. Schmidt, S.A. Corcelli, J.L. Skinner, J. Chem. Phys. 121 (2004) 8887.
[41] T. Hayashi, W. Zhuang, S. Mukamel, J. Phys. Chem. A 109 (2005) 9747.
[42] T.l.C. Jansen, A.G. Dijkstra, T.M. Watson, J.D. Hirst, J. Knoester, J. Chem. Phys. 125 (2006) 44312.
[43] W. Zhuang, D. Abramavicius, T. Hayashi, S. Mukamel, J. Phys. Chem. B 110 (2006) 3362.
[44] T.l.C. Jansen, J. Knoester, J. Chem. Phys. 124 (2006) 44502.
[45] M.J. Frisch et al., Gaussian 03, Rev C.02, Gaussian, Inc., Wallingford CT, 2004.
[46] A.D. MacKerell et al., J. Phys. Chem. B 102 (1998) 3586.
[47] J.C. Phillips, R. Braun, W. Wang, J. Gumbart, E. Tajkhorshid, E. Villa, C. Chipot, R.D. Skeel, L. Kale, K. Schulten, J. Comput. Chem. 26 (2005) 1781.
[48] W.F. Vangunsteren, H.J.C. Berendsen, Mol. Phys. 34 (1977) 1311.
[49] D. Abramavicius, W. Zhuang, S. Mukamel, J. Phys. B: At. Mol. Opt. Phys. 39 (2006) 5051.
[50] S. Mukamel, D. Abramavicius, Chem. Rev. 104 (2004) 2073.
[51] V. Pajcini, S.A. Asher, J. Am. Chem. Soc. 121 (1999) 10942.
[52] D-H. Chin, R.W. Woody, C.A. Rohl, R.L. Baldwin, Proc. Natl. Acad. Sci. USA 99 (2002) 15416.
[53] D. Thouless, Phys. Rep. 13 (1974) 93.